UNIVERSITÀ DEGLI STUDI DI PADOVA

Università degli Studi di Padova

Padua Research Archive - Institutional Repository

Light sterile neutrinos and inflationary freedom

(Article begins on next page)

Light sterile neutrinos and inflationary freedom

S. Gariazzo,[a,b] C. Giunti[b] and M. Laveder[c]

[a]Department of Physics, University of Torino,
  Via P. Giuria 1, I–10125 Torino, Italy
[b]INFN, Sezione di Torino,
  Via P. Giuria 1, I–10125 Torino, Italy
[c]Dipartimento di Fisica e Astronomia "G. Galilei", Università di Padova,
  and INFN, Sezione di Padova,
  Via F. Marzolo 8, I–35131 Padova, Italy

  E-mail: gariazzo@to.infn.it, giunti@to.infn.it, laveder@pd.infn.it

Abstract. We perform a cosmological analysis in which we allow the primordial power spectrum of scalar perturbations to assume a shape that is different from the usual power-law predicted by the simplest models of cosmological inflation. We parameterize the free primordial power spectrum with a "piecewise cubic Hermite interpolating polynomial" (`PCHIP`). We consider a 3+1 neutrino mixing model with a sterile neutrino having a mass at the eV scale, which can explain the anomalies observed in short-baseline neutrino oscillation experiments. We find that the freedom of the primordial power spectrum allows to reconcile the cosmological data with a fully thermalized sterile neutrino in the early Universe. Moreover, the cosmological analysis gives us some information on the shape of the primordial power spectrum, which presents a feature around the wavenumber $k = 0.002\,\mathrm{Mpc}^{-1}$.

JCAP04(2015)023

Contents

1 Introduction

In typical analyses of cosmological data one of the main assumptions about the early Universe is the form of the primordial power-spectrum (PPS) of scalar fluctuations. The PPS is usually assumed to be a power-law (PL), as predicted by the simplest models of inflation (see refs. [1–3]). However, if inflation is generated by a more complicated mechanism, the PPS can assume a different shape or present various features with respect to the power-law form (see refs. [4, 5] and references therein). Since we cannot test directly the physics at the scale of cosmological inflation in order to check the correctness of the simplest inflationary models, any cosmological analysis performed assuming a power-law PPS can suffer of a biased constraint.

The cosmological observable that we can access is the late-time power spectrum of scalar perturbations, which is a convolution of the PPS and the transfer function, that can be calculated numerically as a function of a small number of cosmological parameters. Several experiments are designed to measure the late-time power spectrum at different redshifts (see refs. [6–8]).

The physics of the transfer function is well understood and the experiments that measure the Cosmic Microwave Background (CMB) radiation give very strong constraints on the values of the cosmological parameters which determine the transfer function. The current most precise measurements of the angular power spectrum of the CMB are those of the Planck experiment [9] for the unpolarized data and those of the WMAP experiment [10] for the polarization spectra. However, the next Planck data release is expected to improve the current sensitivity on the unpolarized spectra and to include the new polarized spectra obtained by Planck.

On the other hand, since the inflationary scale cannot be directly tested, we can only try to reconstruct indirectly the PPS. In the literature there are several approaches for reconstructing a completely unknown PPS given the available experimental data. Among them we can list the "cosmic inversion" methods [11–15], maximum entropy deconvolution [16]

and regularization methods like Richardson-Lucy iteration [17–20], truncated singular value decomposition [21] and Tikhonov regularization [22].

The effects on cosmological parameter estimation of considering a PPS which is different from a power-law has been studied in several works: for example, the power-law PPS has been simply modified with the introduction of a running in the tilt of the power-law [23–26], a running of the running [27], or a sharp cut-off in the power-law [26]. Our main goal is to study how the freedom of the form of the PPS can affect the existing bounds on the presence in the early Universe of additional sterile neutrinos. In particular, we want to explore the impact of a light sterile neutrino with mass $m_s \sim 1\,\mathrm{eV}$ which has been thermalized by neutrino oscillations before neutrino decoupling at a temperature of the order of $1\,\mathrm{MeV}$ [28, 29]. Previous analyses of the cosmological data with a standard power-law PPS have found that the case of a fully thermalized sterile neutrino is quite disfavored [30–35]. This result motivated the study of mechanisms which can suppress the thermalization of sterile neutrinos in the early Universe due to active-sterile oscillations before neutrino decoupling [28, 29]. Examples are a large lepton asymmetry [36–40], an enhanced background potential due to new interactions in the sterile sector [41–47], a larger cosmic expansion rate at the time of sterile neutrino production [48], and MeV dark matter annihilation [49].

Besides our main objective, which is to find out how the constraints on the presence in the early Universe of additional sterile neutrinos change if the PPS is not forced to be a power-law, we are also interested in obtaining information on the form of the PPS. With these aims, we considered a general form of the PPS that allows the presence of features without forcing a particular shape. In the literature several model-independent parameterizations have been used: for example, a free PPS can be described with wavelets [50–53], principal components [54], top-hat bins without interpolation [55], power-law bins [56, 57], linear interpolation [25, 58–64], broken power-law [57, 65], and interpolating spline functions [26, 66–72]. We decided to follow part of the prescriptions of the interpolating spline form presented in refs. [69, 71], improving the parametrization by using a "piecewise cubic Hermite interpolating polynomial" (PCHIP), which is described in appendix A. This method allows us to avoid the spurious oscillating behavior that can appear between the nodes of interpolating splines.

This article is structured as follows: in section 2 we introduce the neutrino mixing scheme, the cosmological model and the cosmological data used in the paper, in section 3 and in section 4 we discuss the results obtained from the analysis for the cosmological parameters and for the PPS respectively, and in section 5 we present our conclusions.

2   Neutrino mixing scheme, cosmological model and data

In this section we introduce the models and the datasets used in this paper. In subsection 2.1 we present the neutrino mixing scheme, in subsection 2.2 we introduce the cosmological model, and in subsection 2.3 we present the cosmological data used in our analysis.

2.1   Neutrino mixing scheme

In this paper we consider the 3+1 neutrino mixing scheme, which is motivated by indications in favor of short-baseline neutrino oscillations found in the LSND experiment [73], in Gallium experiments [74–78] and in reactor experiments [79–81]. In this scheme, besides the three standard active flavor neutrinos ν_e, ν_μ, ν_τ, there is a sterile neutrino which does not interact through standard weak interactions. This sterile neutrino is a new particle beyond the Standard Model which cannot be detected directly in current experiments (see [82–84]).

The four flavor neutrinos ν_e, ν_μ, ν_τ, ν_s are superpositions of four massive neutrinos, ν_1, ν_2, ν_3, ν_4 with respective masses m_1, m_2, m_3, m_4. The squared mass differences $\Delta m_{21}^2 \simeq 8 \times 10^{-5}\,\mathrm{eV}^2$ and $\Delta m_{31}^2 \simeq 2 \times 10^{-3}\,\mathrm{eV}^2$ (where $\Delta m_{kj}^2 = m_k^2 - m_j^2$) generate the neutrino oscillations which have been observed in many solar, atmospheric and long-baseline experiments (see [85–88]). An additional much larger squared mass difference $\Delta m_{41}^2 \sim 1\,\mathrm{eV}^2$ is required in order to explain the indications in favor of short-baseline oscillations [89–95]. In the 3+1 scheme the three standard active flavor neutrinos ν_e, ν_μ, ν_τ are mainly composed of the three massive neutrinos ν_1, ν_2, ν_3, but they have a small component of ν_4 in order to generate the observed short-baseline oscillations through Δm_{41}^2. On the other hand, the sterile neutrino ν_s is mainly composed of the massive neutrino ν_4 and in the following we use the common notation $m_s = m_4$.

Since the case of a very light ν_4 and almost degenerate ν_1, ν_2, ν_3 at the eV scale is strongly disfavored by cosmological data (see ref. [96]) we consider the case of $m_s = m_4 \sim 1\,\mathrm{eV}$ and much lighter ν_1, ν_2, ν_3.

The combined analysis of cosmological data and short-baseline neutrino oscillation data is performed by using the posterior distribution of $m_s = m_4 \simeq \sqrt{\Delta m_{41}^2}$ obtained from the analysis of SBL data [95] as a prior in the CosmoMC analysis of cosmological data [31, 33, 34, 97, 98]. As shown in table 3 of ref. [33], the best-fit value of m_s obtained from short-baseline neutrino oscillation data is $1.27\,\mathrm{eV}$ and its 95.45% probability range (2σ) is between 0.97 and $1.42\,\mathrm{eV}$.

2.2 Cosmological model

We used an extended flat ΛCDM model to accommodate the presence of a sterile neutrino and inflationary freedom in the production of the primordial power spectra.

In the analysis with a power-law PPS we consider a flat ΛCDM+ν_s cosmological model with a total of eight parameters:

$$\boldsymbol{\theta} = \{\omega_{\mathrm{cdm}}, \omega_{\mathrm{b}}, \theta_{\mathrm{s}}, \tau, \ln(10^{10} A_s), n_s, m_s, \Delta N_{\mathrm{eff}}\}, \tag{2.1}$$

where $\omega_{\mathrm{cdm}} \equiv \Omega_{\mathrm{cdm}} h^2$ and $\omega_{\mathrm{b}} \equiv \Omega_{\mathrm{b}} h^2$ are the present-day physical CDM and baryon densities, θ_{s} the angular the sound horizon, τ the optical depth to reionisation, and $\ln(10^{10} A_s)$ and n_s denote respectively the amplitude and spectral index of the initial scalar fluctuations at the pivot scale of $0.002\,\mathrm{Mpc}^{-1}$. $\Delta N_{\mathrm{eff}} = N_{\mathrm{eff}} - N_{\mathrm{eff}}^{\mathrm{SM}}$, where $N_{\mathrm{eff}}^{\mathrm{SM}} = 3.046$ [99] is the effective number of relativistic degrees of freedom before photon decoupling in the Standard Model with three massless neutrinos (see [100, 101]).

In contrast with previous analyses [33, 34, 98], we limit the allowed range of ΔN_{eff} in the interval $0 \leq \Delta N_{\mathrm{eff}} \leq 1$, assuming that the additional sterile neutrino cannot contribute to the relativistic energy density more than a standard active neutrino. This happens if sterile neutrinos are produced in the early Universe by neutrino oscillations before neutrino decoupling [28, 29].

We assume a flat prior for all the parameters in eq. (2.1), except m_s, for which we use a flat prior for $0 \leq m_s/\mathrm{eV} \leq 3$ only in the analyses which do not take into account the constraints from short-baseline neutrino oscillation data. In the analyses which take into account these constraints we use as prior for m_s the posterior obtained from the analysis of SBL data presented in ref. [95], as explained at the end of subsection 2.1. We neglect the masses of the three light neutrinos ν_1, ν_2, ν_3, which are assumed to be much smaller than $1\,\mathrm{eV}$.

In order to parameterize a free PPS we follow partially the prescriptions described in [69, 71], but instead of the cubic spline function we interpolate with a "piecewise cubic Hermite interpolating polynomial" (PCHIP) [102, 103], that is described only by the values of the PPS in a discrete number of nodes, as discussed in appendix A. We used 12 nodes which span a wide range of k values:

$$
\begin{aligned}
k_1 &= 5 \times 10^{-6}\,\mathrm{Mpc}^{-1}, \\
k_2 &= 10^{-3}\,\mathrm{Mpc}^{-1}, \\
k_j &= k_2 (k_{11}/k_2)^{(j-2)/9} \quad \text{for} \quad j \in [3, 10], \\
k_{11} &= 0.35\,\mathrm{Mpc}^{-1}, \\
k_{12} &= 10\,\mathrm{Mpc}^{-1}.
\end{aligned}
\tag{2.2}
$$

In the range (k_2, k_{11}), that is well constrained from the data [71], we choose equally spaced nodes in the logarithmic scale. The nodes k_1 and k_{12} are used to parameterize a non-constant behaviour of the PPS outside this range and their position is chosen in order to have all the CosmoMC PPS evaluations inside the interval covered by our parametrization. The PCHIP PPS is described by

$$
P_s(k) = P_0 \times \texttt{PCHIP}(k; P_{s,1}, \ldots, P_{s,12}),
\tag{2.3}
$$

where $P_0 = 2.36 \times 10^{-9}$ [104] and $P_{s,j}$ is the value of the PPS at the node k_j divided by P_0. The function $\texttt{PCHIP}(k; P_{s,1}, \ldots, P_{s,12})$ is described in appendix A.

In the PCHIP PPS analysis we consider a flat ΛCDM$+\nu_s$ cosmological model with a total of 18 parameters:

$$
\boldsymbol{\theta} = \{\omega_{\mathrm{cdm}}, \omega_{\mathrm{b}}, \theta_{\mathrm{s}}, \tau, m_s, \Delta N_{\mathrm{eff}}, P_{s,1}, \ldots, P_{s,12}\},
\tag{2.4}
$$

where $\omega_{\mathrm{cdm}}, \omega_{\mathrm{b}}, \theta_{\mathrm{s}}, \tau, m_s, \Delta N_{\mathrm{eff}}$ are the same as those in the set (2.1). We assume a flat prior on $P_{s,j}$ in the range $0.01 \leq P_{s,j} \leq 10$.

The Bayesian analysis is performed through an appropriately modified version of the Monte Carlo Markov Chain (MCMC) package CosmoMC [105], using the Boltzmann equations solver CAMB [106] (Code for Anisotropies in the Microwave Background) for the calculation of the observables.

2.3 Cosmological data sets

In this paper we use the same dataset as in refs. [34, 98], apart from the controversial BICEP2 data on the B-mode polarization of the CMB [107] that we neglect:

- **CMB** (Cosmic Microwave Radiation): the temperature fluctuations power spectra provided by the Planck satellite [108] up to $\ell = 2479$, by Atacama Cosmology Telescope (ACT) [109] and South Pole Telescope (SPT) [110] whose likelihoods cover the high multipole range, $500 < \ell < 3500$ and $650 < \ell < 3000$, respectively. Concerning polarization we include the data of the Wilkinson Microwave Anisotropy Probe (WMAP) nine year data release [10].

- **LSS** (Large Scale Structure): the matter power spectrum at four different redshifts $z = 0.22$, $z = 0.41$, $z = 0.60$ and $z = 0.78$ from the WiggleZ Dark Energy Survey [7].

- **H_0**: the Hubble parameter as obtained with the Hubble Space Telescope (HST) [111], which acts as a prior on the derived cosmological parameter $H_0 = 73.8 \pm 2.4 \, \mathrm{km \, s^{-1} \, Mpc^{-1}}$.

- **PSZ**: the Planck Sunayev Zel'Dovich catalogue [112] contains 189 galaxy clusters identified through the Sunayev Zel'Dovich effect. The number counts allows to compute the cluster mass function, which is related to a combination of Ω_m and σ_8: $\sigma_8(\Omega_m/0.27)^{0.3} = 0.782 \pm 0.010$. This result contributes as an additional χ^2 in our analysis.

- **CFHTLenS**: the 2D cosmic shear correlation function as determined by the Canada-France Hawaii Telescope Lensing Survey (CFHTLenS) [113, 114] through the measurements of redshifts and shapes of 4.2 million galaxies spanning the range $0.2 < z < 1.3$. The weak gravitational lensing signal extracted from these measurements constrains a combination of the total matter density and the standard deviation of the amplitude of the matter density fluctuations on a sphere of radius $8h^{-1}$Mpc: $\sigma_8(\Omega_m/0.27)^{0.46} = 0.774 \pm 0.040$. This result is incorporated in our analysis following the same prescription used for PSZ.

In the following we denote the analyses of all these cosmological data alone as "COSMO" and those which include also the short-baseline neutrino oscillation prior as "COSMO+SBL".

3 Cosmological parameters and sterile neutrinos

The results of our COSMO and COSMO+SBL analyses are presented in table 1 for the standard case of a power-law PPS and in table 2 for the free PPS with the PCHIP parameterization. In the upper part of the tables we listed the common parameters of the ΛCDM model, in the central part we listed the neutrino parameters ΔN_{eff} and m_s, while the lower part concerns the parameters used to parameterize the PPS: n_s and $\log(10^{10} A_s)$ for the power-law PPS and $P_{s,j}$ for the PCHIP PPS. The constraints on the PPS parameters are discussed in the next section. In this section we discuss first the results relative to the parameters in the upper part of the tables, $100 \, \Omega_b h^2$, $\Omega_{\mathrm{cdm}} h^2$, θ_s and τ, and then the results relative to the parameters in the central part of the tables, ΔN_{eff} and m_s.

The bounds on the parameters of the ΛCDM model change slightly when more freedom is admitted for the PPS. Comparing tables 1 and 2, one can see that the limits on the parameters of the ΛCDM model are slightly weakened in the PCHIP PPS case and for some parameters there is also a small shift in the marginalized best-fit value. In all the cases in which this happens, the marginalized best-fit values move inside the 1σ uncertainties. The freedom of the form of the PPS affects the COSMO results more than the COSMO+SBL results: in the former case the $\Omega_{\mathrm{cdm}} h^2$ and θ_s best values change by about 1σ, while a smaller shift is obtained for $100 \, \Omega_b h^2$. On the other hand, in the COSMO+SBL analysis all the shifts are much smaller than the 1σ uncertainties.

Figure 1 shows the marginalized 1σ, 2σ and 3σ allowed intervals for ΔN_{eff} and m_s that we obtained in the COSMO(PL) and COSMO(PCHIP) analyses, without the SBL prior. Figure 2 shows the corresponding marginalized 1σ, 2σ and 3σ allowed regions in the m_s–ΔN_{eff} plane. We can notice some major changes in the allowed values of both ΔN_{eff} and m_s in the PCHIP PPS case with respect to the power-law PPS case. With a power-law PPS the best-fit value of ΔN_{eff} is around 0.4, whereas with the PCHIP PPS it is at $\Delta N_{\mathrm{eff}} = 1$,

Parameters	COSMO	COSMO+SBL
$100\,\Omega_{\rm b}h^2$	$2.263^{+0.026\ +0.052\ +0.078}_{-0.027\ -0.053\ -0.080}$	$2.251^{+0.023\ +0.049\ +0.075}_{-0.025\ -0.045\ -0.067}$
$\Omega_{\rm cdm}h^2$	$0.120^{+0.004\ +0.008\ +0.011}_{-0.005\ -0.008\ -0.009}$	$0.117^{+0.002\ +0.006\ +0.010}_{-0.003\ -0.005\ -0.006}$
$\theta_{\rm s}$	$1.0412^{+0.0007\ +0.0014\ +0.0020}_{-0.0007\ -0.0014\ -0.0021}$	$1.0416^{+0.0006\ +0.0012\ +0.0018}_{-0.0006\ -0.0012\ -0.0019}$
τ	$0.087^{+0.013\ +0.028\ +0.045}_{-0.014\ -0.026\ -0.037}$	$0.087^{+0.013\ +0.026\ +0.040}_{-0.013\ -0.025\ -0.035}$
$\Delta N_{\rm eff}$	$0.38^{+0.18}_{-0.33}$; No limit; No limit	$0.19^{+0.09}_{-0.12}$; < 0.41; < 0.60
$m_s[\mathrm{eV}]$	$0.61^{+0.31}_{-0.42}$; < 2.03; No limit	$1.25^{+0.11\ +0.17\ +0.22}_{-0.16\ -0.29\ -0.35}$
$n_{\rm s}$	$0.979^{+0.011\ +0.020\ +0.030}_{-0.010\ -0.020\ -0.025}$	$0.969^{+0.005\ +0.011\ +0.017}_{-0.005\ -0.011\ -0.016}$
$\log(10^{10}A_s)$	$3.152^{+0.031\ +0.064\ +0.094}_{-0.032\ -0.058\ -0.087}$	$3.178^{+0.024\ +0.048\ +0.072}_{-0.025\ -0.051\ -0.075}$

Table 1. Marginalized 1σ, 2σ and 3σ confidence level limits for the cosmological parameters obtained with the power-law parametrization for the PPS.

Parameters	COSMO	COSMO+SBL
$100\,\Omega_{\rm b}h^2$	$2.251^{+0.036\ +0.073\ +0.111}_{-0.036\ -0.073\ -0.110}$	$2.247^{+0.036\ +0.072\ +0.111}_{-0.038\ -0.078\ -0.117}$
$\Omega_{\rm cdm}h^2$	$0.125^{+0.005\ +0.007\ +0.009}_{-0.004\ -0.011\ -0.014}$	$0.118^{+0.004\ +0.011\ +0.016}_{-0.005\ -0.007\ -0.008}$
$\theta_{\rm s}$	$1.0407^{+0.0007\ +0.0016\ +0.0024}_{-0.0008\ -0.0014\ -0.0020}$	$1.0413^{+0.0008\ +0.0014\ +0.0020}_{-0.0007\ -0.0016\ -0.0024}$
τ	$0.086^{+0.014\ +0.033\ +0.053}_{-0.016\ -0.028\ -0.038}$	$0.090^{+0.014\ +0.033\ +0.051}_{-0.016\ -0.029\ -0.039}$
$\Delta N_{\rm eff}$	> 0.54; No limit; No limit	$0.25^{+0.13}_{-0.22}$; < 0.75; No limit
$m_s[\mathrm{eV}]$	$0.62^{+0.21\ +0.87}_{-0.26\ -0.54}$; No limit	$1.22^{+0.13\ +0.17\ +0.24}_{-0.15\ -0.28\ -0.33}$
$P_{s,1}$	< 2.51; < 8.13; No limit	< 2.75; < 8.30; No limit
$P_{s,2}$	$1.06^{+0.19\ +0.43\ +0.71}_{-0.22\ -0.35\ -0.43}$	$1.05^{+0.18\ +0.44\ +0.75}_{-0.22\ -0.35\ -0.44}$
$P_{s,3}$	$0.65^{+0.19\ +0.38\ +0.57}_{-0.19\ -0.37\ -0.54}$	$0.67^{+0.20\ +0.39\ +0.61}_{-0.19\ -0.36\ -0.52}$
$P_{s,4}$	$1.14^{+0.11\ +0.23\ +0.36}_{-0.11\ -0.22\ -0.31}$	$1.13^{+0.11\ +0.23\ +0.34}_{-0.11\ -0.21\ -0.31}$
$P_{s,5}$	$0.97^{+0.06\ +0.11\ +0.17}_{-0.05\ -0.10\ -0.16}$	$0.98^{+0.05\ +0.11\ +0.17}_{-0.06\ -0.10\ -0.15}$
$P_{s,6}$	$0.96^{+0.03\ +0.07\ +0.10}_{-0.03\ -0.06\ -0.08}$	$0.98^{+0.03\ +0.07\ +0.11}_{-0.03\ -0.06\ -0.08}$
$P_{s,7}$	$0.94^{+0.03\ +0.06\ +0.10}_{-0.03\ -0.05\ -0.07}$	$0.94^{+0.03\ +0.06\ +0.10}_{-0.03\ -0.06\ -0.07}$
$P_{s,8}$	$0.93^{+0.03\ +0.06\ +0.10}_{-0.03\ -0.05\ -0.07}$	$0.93^{+0.03\ +0.06\ +0.10}_{-0.03\ -0.06\ -0.07}$
$P_{s,9}$	$0.93^{+0.03\ +0.07\ +0.11}_{-0.03\ -0.06\ -0.08}$	$0.91^{+0.03\ +0.07\ +0.10}_{-0.03\ -0.06\ -0.07}$
$P_{s,10}$	$0.91^{+0.04\ +0.08\ +0.12}_{-0.04\ -0.08\ -0.11}$	$0.88^{+0.03\ +0.08\ +0.14}_{-0.04\ -0.07\ -0.08}$
$P_{s,11}$	$1.14^{+0.17\ +0.28\ +0.42}_{-0.16\ -0.30\ -0.39}$	$1.00^{+0.13\ +0.35\ +0.52}_{-0.17\ -0.24\ -0.28}$
$P_{s,12}$	< 0.70; < 1.19; < 1.54	< 0.49; < 1.01; < 1.33

Table 2. Marginalized 1σ, 2σ and 3σ confidence level limits for the cosmological parameters obtained with the PCHIP parametrization for the PPS.
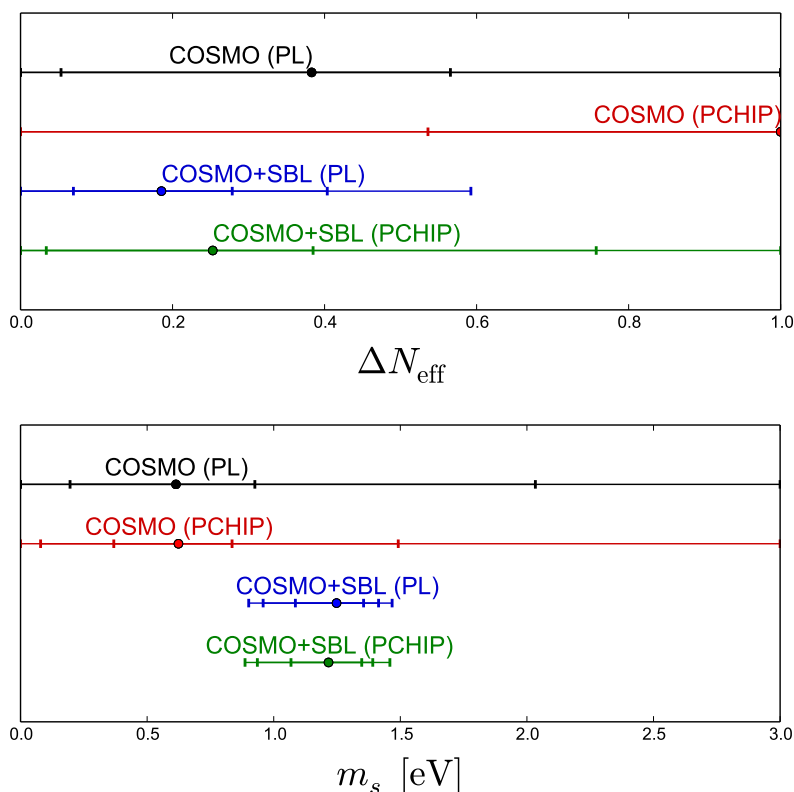
Figure 1. 1σ, 2σ and 3σ marginalized intervals for $\Delta N_{\rm eff}$ and m_s obtained in the different analyses discussed in the text (considering $0 \le \Delta N_{\rm eff} \le 1$ and $0 \le m_s/{\rm eV} \le 3$).

that is the upper limit for $\Delta N_{\rm eff}$ assumed in the analysis. The reason of this behavior is that the effects of the presence of additional relativistic energy in the primordial universe can be compensated by an increase of the PCHIP PPS at large k. As a result, the marginalized posterior for $\Delta N_{\rm eff}$ is increased in the region towards $\Delta N_{\rm eff} = 1$, in correspondence with higher values in the PCHIP PPS for $k > 0.35\,{\rm Mpc}^{-1}$.

Without the SBL constraint on m_s, the different preferences for the value of $\Delta N_{\rm eff}$ in the power-law and PCHIP PPS analyses correspond to different allowed intervals for m_s. As shown in figure 1, although in both cases the best-fit value of m_s is near $0.6\,{\rm eV}$, the intermediate preferred region for $\Delta N_{\rm eff}$ in the power-law PPS analysis gives for m_s an upper limit of about $2\,{\rm eV}$ at 2σ, whereas the large preferred values for $\Delta N_{\rm eff}$ in the PCHIP PPS analysis gives a tighter upper limit of about $1.5\,{\rm eV}$ at 2σ.

The SBL prior on the sterile neutrino mass m_s puts a constraint so strong that in practice the value of this parameter does not depend on the inclusion or not of the freedom of the PPS. In fact, the m_s limits in tables 1 and 2 are similar in the power-law PPS and PCHIP PPS analyses. This can be seen also from the marginalized allowed intervals of m_s in figure 1, comparing the COSMO+SBL(PL) and COSMO+SBL(PCHIP) allowed intervals.

A major difference occurs, instead, in the limits for $\Delta N_{\rm eff}$, because the effects of the presence of additional relativistic energy in the primordial universe can be compensated by an increase in the PCHIP PPS at large k, as in the case without the SBL constraint on m_s. As shown in figure 1, the best-fit and upper limits on $\Delta N_{\rm eff}$ in the COSMO+SBL(PL) and

COSMO+SBL(PCHIP) are different. In particular, in the COSMO+SBL(PCHIP) the 3σ upper limit on $\Delta N_{\rm eff}$ allows the presence of a fully thermalized sterile neutrino compatible with the SBL constraint on m_s.

Figure 3 shows the contour plots of the marginalized 1σ, 2σ and 3σ regions in the m_s–$\Delta N_{\rm eff}$ plane that we obtained in the COSMO+SBL(PL) and COSMO+SBL(PCHIP) analyses. The allowed regions in the left panel are similar[1] to those obtained in ref. [34] with a standard power-law PPS. One can see that in this case a fully thermalized sterile neutrino is quite disfavored. On the other hand, from the right panel one can see that in the PCHIP PPS analysis a fully thermalized sterile neutrino with a mass just below 1 eV and with $\Delta N_{\rm eff} = 1$ is even inside the 2σ region. This means that a fully thermalized sterile neutrino can be accommodated in the cosmological model if the PPS is not forced to be described by a power-law.

4   Best-fitting primordial power spectrum

The results of our PCHIP PPS analyses without and with the SBL prior on m_s give interesting information on the shape of the PPS.

The marginalized posterior limits for the values $P_{s,j}$ in eq. (2.3) are listed in table 2. One can see that the least constrained nodes are the first and last, in k_1 and k_{12}, for which there are only upper limits on the corresponding $P_{s,j}$. This was expected, because there are no data at the edges of the wide interval of k that we have considered. For these two extreme nodes the marginalized posterior is peaked on the lowest value that we allowed in the fit (0.01).

On the contrary, the nodes from 5 to 10 are well constrained, at the level of a few percent at 1σ. Considering the nodes from 2 to 4, one can see that the second node has preferred values higher than 1 within 1σ, the third node value is more than 2σ below 1 (around 0.6), the fourth node value is again higher than 1 at more than 1σ. This implies that the PPS that we obtained from the MCMC has a significant dip around $k_3 \simeq 0.002\,{\rm Mpc}^{-1}$ and a less significant bump around $k_4 \simeq 0.0035\,{\rm Mpc}^{-1}$.

To help the reader to visualize this feature, we present in figure 4 a comparison of the best-fitting PPS[2] in the power-law parametrization and in the PCHIP parametrization, without and with the SBL constraint. One can see that the best-fitting PCHIP curves with and without the SBL prior are significantly different only for $k \gtrsim k_{10}$. The dip around $k_3 \simeq 0.002\,{\rm Mpc}^{-1}$ and the bump around $k_4 \simeq 0.0035\,{\rm Mpc}^{-1}$ are clearly seen in the PCHIP parametrization.

From figure 4 one can also see that the PCHIP parametrization has an approximate power-law behavior between about $k_5 \simeq 0.007\,{\rm Mpc}^{-1}$ and $k_{10} \simeq 0.2\,{\rm Mpc}^{-1}$.

Another helpful way to visualize the behaviour of the PPS obtained in the analyses without and with the SBL prior with the PCHIP parametrization is presented in figure 5,

---

[1]The only difference is that the analysis in ref. [34] took into account also the BICEP2 data on the B-mode polarization of the CMB [107].

[2]We consider as the best-fitting PPS that which corresponds to the lower value $\chi^2_{\rm min}$ of $\chi^2 = -2\ln\mathcal{P}$, where $\mathcal{P}$ is the marginalized posterior probability in the space of the parameters $P_{s,1}, \ldots, P_{s,12}$. However, one must take into account that in a parameter space with a large number of dimensions $N_{\rm P}$ the MCMC is not expected to explore well the region near the true global best-fit corresponding to $\chi^2_{\rm min,true}$. In fact, the points are distributed mainly in a region where $\chi^2 - \chi^2_{\rm min,true} \sim N_{\rm P}$. Therefore, the PPS that we consider as best-fitting can be different from the true best-fitting PPS in the intervals of k which are not well constrained by the data.
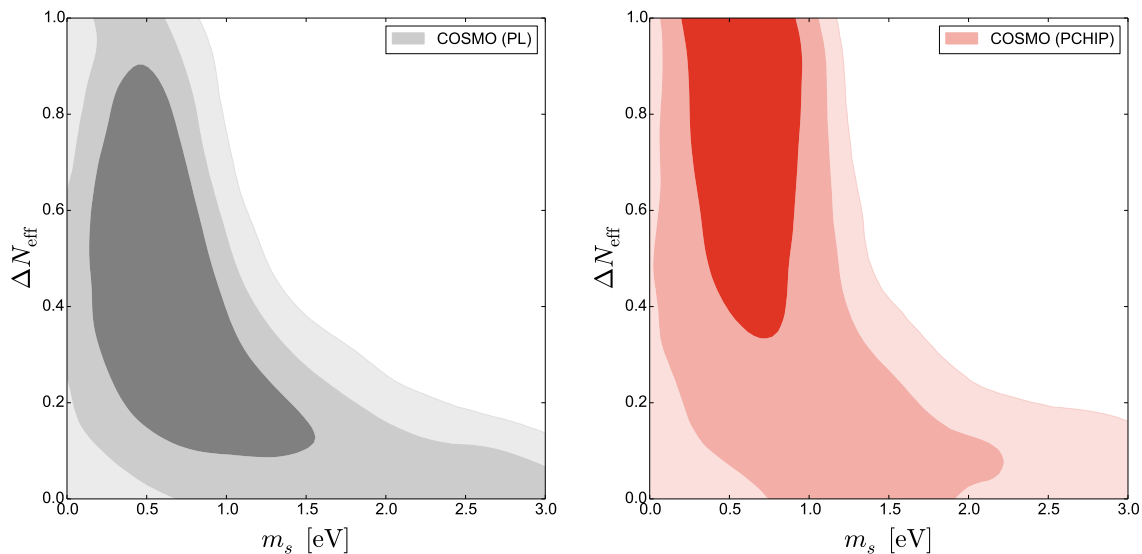
Figure 2. 1σ, 2σ and 3σ marginalized contours in the $m_s - \Delta N_{\mathrm{eff}}$ plane in the fits without the SBL prior. The left and right panels correspond, respectively, to the standard power-law PPS and the PCHIP PPS analyses.
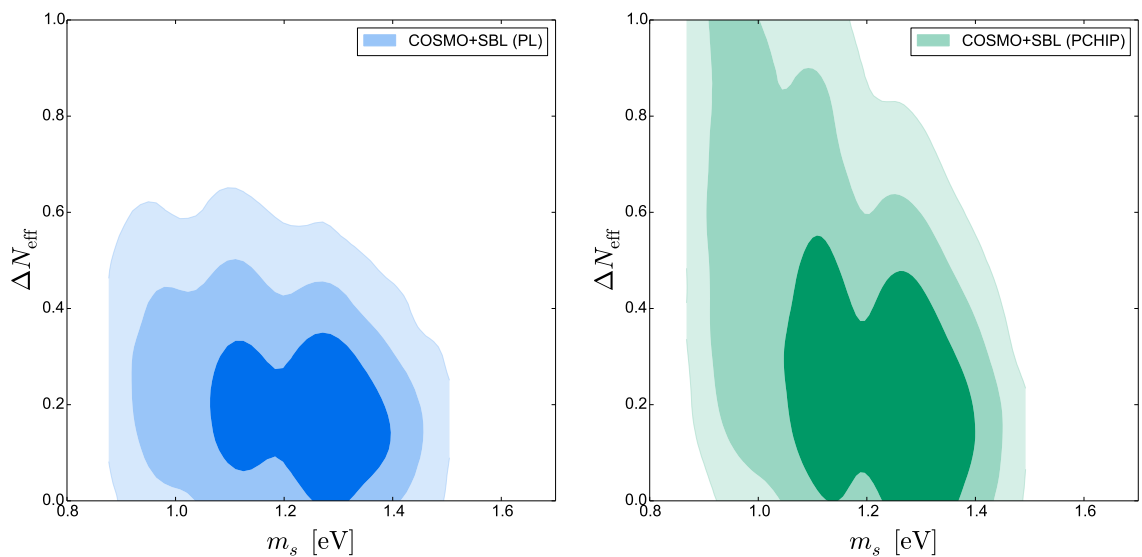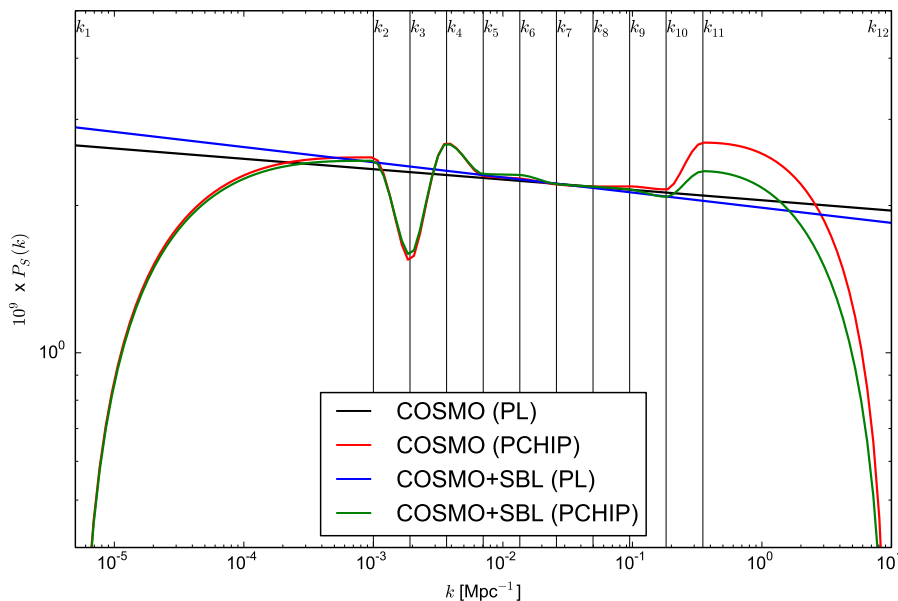

Figure 3. 1σ, 2σ and 3σ marginalized contours in the $m_s - \Delta N_{\mathrm{eff}}$ plane in the fits with the SBL prior. The left and right panels correspond, respectively, to the standard power-law PPS and the PCHIP PPS analyses.

Figure 4. Best-fit PPS with different dataset combinations and PPS parameterizations.

which shows the 1σ, 2σ and 3σ bands obtained by marginalizing the posterior distribution for each value of the wavenumber k in a fine grid. The two plots in figure 5 show a well collimated band corresponding to the region in which the power-law gives a good approximation of the PCHIP PPS, between about $k_5 \simeq 0.007\,\mathrm{Mpc}^{-1}$ and $k_{10} \simeq 0.2\,\mathrm{Mpc}^{-1}$. Moreover, the dip at $k \simeq 0.002\,\mathrm{Mpc}^{-1}$ is well visible, as well as the bump at $k \simeq 0.0035\,\mathrm{Mpc}^{-1}$. On the other hand, the widths of the bands diverge for low and high values of k, where there are large uncertainties.

The major features that we have noticed in the reconstructed PPS are in agreement with those found in ref. [20], in which the scalar PPS has been reconstructed with a totally different technique, the Richardson-Lucy iteration algorithm, using the transfer function corresponding to the Planck 2013 best-fit for the ΛCDM model. Apart for the suppression that they found around $k \simeq 2\times10^{-4}\,\mathrm{Mpc}^{-1}$ and the features at higher k, the main differences with respect to the power-law PPS are the same that we found in our analysis. According to the authors of ref. [20], these major features are related to the low-ℓ spectrum of the temperature perturbations measured by the Planck experiment, that obtained a dip in the power around $\ell \simeq 22$ and a slight excess around $\ell \simeq 40$.

Although the parametrization with a natural cubic spline is noisy due to spurious oscillations between the nodes, also in figure 8 of ref. [71] it is possible to guess the presence of a dip around $k \simeq 0.002\,\mathrm{Mpc}^{-1}$, especially in the curves with more than 20 nodes. However, our parametrization is much cleaner and permits a better visualization of these features.
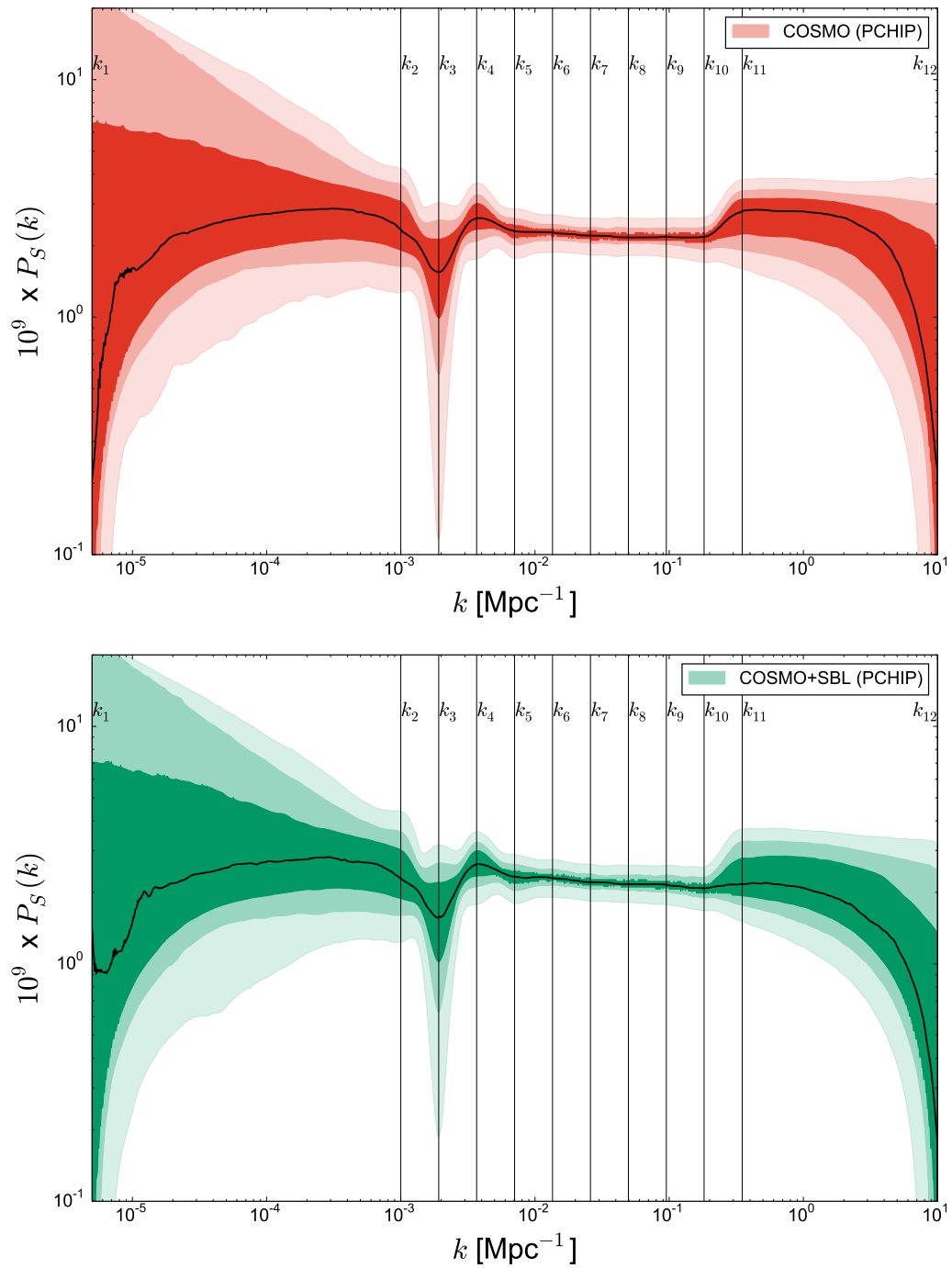
Figure 5. Allowed 1σ, 2σ and 3σ bands of the PCHIP PPS obtained in the analyses without (COSMO) and with (COSMO+SBL) the SBL prior. The bands have been obtained by marginalizing the posterior distribution for each value of the wavenumber k in a fine grid. The black curves correspond to the maximum of the posterior distribution for each value of k.

5 Conclusions

In this work we analyzed the effects of a free form of the primordial power-spectrum of scalar fluctuations, which is not constrained to the usual power-law form that is predicted by the simplest models of inflation (see refs. [1–3]). This freedom in the PPS could arise from a more complicate inflationary mechanism (see refs. [4, 5] and references therein).

We parameterized the PPS with a "piecewise cubic Hermite interpolating polynomial" (PCHIP) described in details in appendix A. Our PCHIP parameterization of the PPS depends from the values of the PPS in twelve nodes (given in eq. (2.2)) which cover a wide range of values of the wavenumber k. We choose the PCHIP method in order to avoid spurious oscillations of the interpolated function between the nodes that can be obtained with spline interpolations (see refs. [69, 71]).

We performed an analysis of cosmological data in which only the primordial spectrum of scalar perturbations is considered, neglecting the controversial [96, 115] data on the B-mode polarization of the CMB [107] which would require to take into account also the primordial spectrum of tensor perturbations. We used the most precise CMB measurements together with low-redshift measurements of the Hubble parameter, the galaxy distribution and the matter distribution in the Universe (see section 2.3).

We found that the freedom of the form of the PPS does not affect significantly the fitted values of the parameters in the ΛCDM model, while the results concerning the existence of a sterile neutrino in the early Universe can change drastically. If we do not impose any prior on the sterile neutrino mass m_s from the results of short-baseline oscillation experiments (see section 2.1), a larger value for the sterile neutrino contribution ΔN_{eff} to the effective number of relativistic degrees of freedom before photon decoupling is preferred in the PCHIP PPS parameterization with respect to the standard power-law parameterization. The marginalized best fit of ΔN_{eff} is moved towards one, which corresponds to a fully thermalized sterile neutrino. This shift corresponds to a tightening of the cosmological preferred values for m_s.

In the analysis with a prior on m_s obtained from the fit of short-baseline oscillation experiments [95], the freedom of the PCHIP PPS affects only the bound on ΔN_{eff}, because the allowed range of m_s is strongly constrained by the SBL prior. We found that a free form of the PPS allows the existence in the early Universe of a fully thermalized sterile neutrino with a mass of about $1\,\mathrm{eV}$ [28, 29]. This possibility is quite disfavored by the analysis of cosmological data with a power-law PPS [30–35]. Hence, the freedom of the PPS allows us to reconcile the cosmological data with short-baseline neutrino oscillations without the need of an additional mechanism which suppresses the thermalization of the sterile neutrino [36–49].

We obtained also some interesting information on the form of the PPS, whose behavior is well constrained by the cosmological analysis for $0.001\,\mathrm{Mpc}^{-1} \lesssim k \lesssim 0.3\,\mathrm{Mpc}^{-1}$. In particular, we have shown that in the range $0.007\,\mathrm{Mpc}^{-1} \lesssim k \lesssim 0.2\,\mathrm{Mpc}^{-1}$ the PPS can be approximated with a power-law and the values of the PPS in the nodes of the PCHIP parameterization lying in this range of k have only a few-percent uncertainty. The PPS in the range $0.001\,\mathrm{Mpc}^{-1} \lesssim k \lesssim 0.0035$ presents a clear dip at $k \simeq 0.002\,\mathrm{Mpc}^{-1}$, with a statistical significance of more than 2σ, and a small bump at $k \simeq 0.0035\,\mathrm{Mpc}^{-1}$, with a statistical significance of about 1σ. These features of the PPS are in agreement with those found in ref. [20] with a completely different method.

In the future the analysis presented in this work could be repeated with the inclusion of a parametrization for the primordial spectrum of tensor perturbations when improved data on the B-mode polarization of the CMB will be available. This will allow us to study with more precision the few relics of cosmological inflation that we can access.

Acknowledgments

A `PCHIP` parametrization of the primordial power spectrum

In this work we parameterized the PPS with a "piecewise cubic Hermite interpolating polynomial" (`PCHIP`) [102, 103]. We decided to adopt this interpolating function in order to avoid spurious oscillations of the interpolating function between the nodes which is often obtained in spline interpolations. This problem occurs because a natural cubic spline requires the values of the function, the first and the second derivatives to be continuous in the nodes [116].

The `PCHIP` function, instead, is constructed in order to preserve the shape of the set of points to be interpolated. This is achieved with a modification of the "monotone piecewise cubic interpolation" [102] which can accommodate non-monotone functions and preserves the local monotonicity.

Let us consider a function with known values y_j in N nodes x_j, with $j = 1, \ldots, N$. A piecewise cubic interpolation is performed with $N - 1$ cubic functions between the nodes. The determination of these $N - 1$ cubic functions requires the determination of $4(N - 1)$ coefficients. Besides the $2(N - 1)$ constraints obtained by requiring that the initial and final point of each cubic function match the known values of the original function in the corresponding nodes, one needs a prescription for the other $2(N - 1)$ necessary constraints. In the case of a natural cubic spline interpolation one gets $2(N-2)$ constraints by requiring the continuity of the first and second derivatives in the nodes and the remaining two constraints are obtained by requiring that the second derivatives in the first and last nodes vanish. The drawback of this method is that the interpolating curve is determined by a set of linear equations without any local control. In fact, all the interpolating curve is affected by the change of a single point.

Local control of the interpolating curve can be achieved by relaxing the requirement of continuity of the second derivatives in the nodes and using the resulting freedom to adjust the first derivatives with a local prescription. In order to see how it can be done, it is convenient to write the cubic interpolating polynomial between the nodes x_j and x_{j+1} in the Hermite form

$$f(x; y_1, \ldots, y_N) = \frac{(h_j + 2t)\,(h_j - t)^2}{h_j^3} y_j + \frac{(3h_j - 2t)\,t^2}{h_j^3} y_{j+1} + \frac{(h_j - t)^2\,t}{h_j^2} d_j + \frac{t^2\,(h_j - t)}{h_j^2} d_{j+1},$$

$$\text{(A.1)}$$

where $t = x - x_j$ and $h_j = x_{j+1} - x_j$. Here d_j and d_{j+1} are the values of the derivatives in the two nodes. In the `PCHIP` method the derivatives are chosen in order to preserve the local monotonicity of the interpolated points. This is done by considering the relative differences

$$\delta_j = \frac{y_{j+1} - y_j}{x_{j+1} - x_j}. \qquad \text{(A.2)}$$

The `PCHIP` prescription is:

- If δ_{j-1} and δ_j have opposite signs, then x_j is a discrete local minimum or maximum and $d_j = 0$.

- If δ_{j-1} and δ_j have the same sign, then d_j is determined by the weighted harmonic mean

$$\frac{w_1 + w_2}{d_j} = \frac{w_1}{\delta_{j-1}} + \frac{w_2}{\delta_j}, \tag{A.3}$$

with $w_1 = 2h_j + h_{j-1}$ and $w_2 = h_j + 2h_{j-1}$.

- The derivatives in the first and last nodes are determined by a shape-preserving pre-scription based on a quadratic fit of three points. For d_1 we consider the three points (x_1, y_1), (x_2, y_2), (x_3, y_3). The derivative in x_1 of the parabola which passes through these three points is given by

$$d(h_1, h_2, \delta_1, \delta_2) = \frac{(2h_1 + h_2)\,\delta_1 - h_1\delta_2}{h_1 + h_2}\,. \tag{A.4}$$

The shape-preserving prescription for d_1 is:

  - If the signs of $d(h_1, h_2, \delta_1, \delta_2)$ and δ_1 are different, then $d_1 = 0$.
  - If the signs of δ_1 and δ_2 are different and $|d(h_1, h_2, \delta_1, \delta_2)| > 3|\delta_1|$, then $d_1 = 3\delta_1$.
  - Else $d_1 = d(h_1, h_2, \delta_1, \delta_2)$.

For d_N one must replace $1 \to N - 1$ and $2 \to N - 2$.

We fit the power spectrum $P_s(k)$ with eq. (2.3), in which the function $\texttt{PCHIP}(k; P_{s,1}, \ldots, P_{s,12})$ is calculated with the $\texttt{PCHIP}$ prescription in the logarithmic scale of k:

$$\texttt{PCHIP}(k; P_{s,1}, \ldots, P_{s,12}) = f(\log k; P_{s,1}, \ldots, P_{s,12})\,. \tag{A.5}$$

A comparison between the natural cubic spline and the $\texttt{PCHIP}$ interpolations of the PPS is presented in figure 6. We choose the same nodes positions that we used for the PPS parametrization in our cosmological analysis and we choose the values of the function in the nodes in order to show the difference between the natural cubic spline and the $\texttt{PCHIP}$ interpolations. One can see that the $\texttt{PCHIP}$ interpolation can reproduce the shape of the points without adding the spurious features between the points that are clearly visible in the natural cubic spline interpolation.
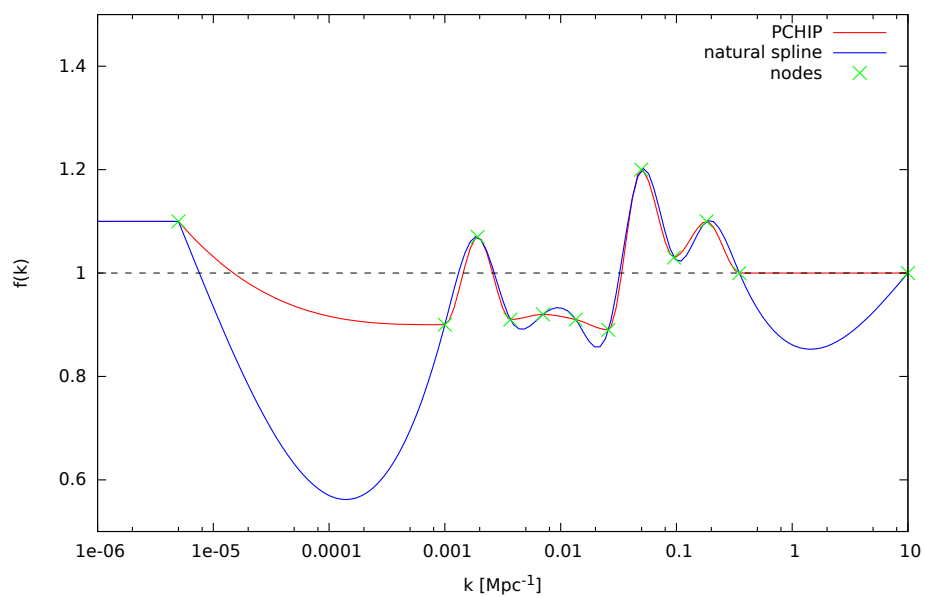
Figure 6. Illustration of the difference between the PCHIP (red line) and the natural spline (blue line) interpolations $f(\log k; y_1, \ldots, y_{12})$ of a function with known values $y_1, \ldots, y_{12}$ in 12 nodes (green crosses) at the values of k in eq. (2.2). The values $y_1, \ldots, y_{12}$ in the nodes are 1.1, 0.9, 1.07, 0.91, 0.92, 0.91, 0.89, 1.2, 1.03, 1.1, 1.0, 1.0.

References

[1] D.H. Lyth and A. Riotto, *Particle physics models of inflation and the cosmological density perturbation*, *Phys. Rept.* **314** (1999) 1 [hep-ph/9807278] [INSPIRE].

[2] B.A. Bassett, S. Tsujikawa and D. Wands, *Inflation dynamics and reheating*, *Rev. Mod. Phys.* **78** (2006) 537 [astro-ph/0507632] [INSPIRE].

[3] D. Baumann and H.V. Peiris, *Cosmological Inflation: Theory and Observations*, *Adv.Sci.Lett.* **2** (2009) 105, 0810.3022 [astro-ph]

[4] J. Martin, C. Ringeval and V. Vennin, *Encyclopædia Inflationaris*, *Phys. Dark Univ.* (2014) [arXiv:1303.3787] [INSPIRE].

[5] N. Kitazawa and A. Sagnotti, *Pre-inflationary clues from String Theory?*, *JCAP* **04** (2014) 017 [arXiv:1402.1418] [INSPIRE].

[6] SDSS collaboration, M. Tegmark et al., *Cosmological parameters from SDSS and WMAP*, *Phys. Rev.* **D 69** (2004) 103501 [astro-ph/0310723] [INSPIRE].

[7] D. Parkinson et al., *The WiggleZ Dark Energy Survey: Final data release and cosmological results*, *Phys. Rev.* **D 86** (2012) 103518 [arXiv:1210.2130] [INSPIRE].

[8] SDSS collaboration, C.P. Ahn et al., *The Ninth Data Release of the Sloan Digital Sky Survey: First Spectroscopic Data from the SDSS-III Baryon Oscillation Spectroscopic Survey*, *Astrophys. J. Suppl.* **203** (2012) 21 [arXiv:1207.7137] [INSPIRE].

[9] PLANCK collaboration, P.A.R. Ade et al., *Planck 2013 results. I. Overview of products and scientific results*, *Astron. Astrophys.* **571** (2014) A1 [arXiv:1303.5062] [INSPIRE].

[10] WMAP collaboration, C.L. Bennett et al., *Nine-Year Wilkinson Microwave Anisotropy Probe (WMAP) Observations: Final Maps and Results*, *Astrophys. J. Suppl.* **208** (2013) 20 [arXiv:1212.5225] [INSPIRE].

[11] M. Matsumiya, M. Sasaki and J. Yokoyama, *Cosmic inversion: Reconstructing primordial spectrum from CMB anisotropy*, *Phys. Rev.* **D 65** (2002) 083007 [astro-ph/0111549] [INSPIRE].

[12] M. Matsumiya, M. Sasaki and J. Yokoyama, *Cosmic inversion. 2. An iterative method for reproducing the primordial spectrum from the CMB data*, *JCAP* **02** (2003) 003 [astro-ph/0210365] [INSPIRE].

[13] N. Kogo, M. Matsumiya, M. Sasaki and J. Yokoyama, *Reconstructing the primordial spectrum from WMAP data by the cosmic inversion method*, *Astrophys. J.* **607** (2004) 32 [astro-ph/0309662] [INSPIRE].

[14] N. Kogo, M. Sasaki and J. Yokoyama, *Constraining cosmological parameters by the cosmic inversion method*, *Prog. Theor. Phys.* **114** (2005) 555 [astro-ph/0504471] [INSPIRE].

[15] R. Nagata and J. Yokoyama, *Reconstruction of the primordial fluctuation spectrum from the five-year WMAP data by the cosmic inversion method with band-power decorrelation analysis*, *Phys. Rev.* **D 78** (2008) 123002 [arXiv:0809.4537] [INSPIRE].

[16] G. Goswami and J. Prasad, *Maximum Entropy deconvolution of Primordial Power Spectrum*, *Phys. Rev.* **D 88** (2013) 023522 [arXiv:1303.4747] [INSPIRE].

[17] A. Shafieloo and T. Souradeep, *Primordial power spectrum from WMAP*, *Phys. Rev.* **D 70** (2004) 043523 [astro-ph/0312174] [INSPIRE].

[18] G. Nicholson and C.R. Contaldi, *Reconstruction of the Primordial Power Spectrum using Temperature and Polarisation Data from Multiple Experiments*, *JCAP* **07** (2009) 011 [arXiv:0903.1106] [INSPIRE].

[19] D.K. Hazra, A. Shafieloo and T. Souradeep, *Cosmological parameter estimation with free-form primordial power spectrum*, *Phys. Rev.* **D 87** (2013) 123528 [arXiv:1303.5336] [inSPIRE].

[20] D.K. Hazra, A. Shafieloo and T. Souradeep, *Primordial power spectrum from Planck*, *JCAP* **11** (2014) 011 [arXiv:1406.4827] [inSPIRE].

[21] G. Nicholson, C.R. Contaldi and P. Paykari, *Reconstruction of the Primordial Power Spectrum by Direct Inversion*, *JCAP* **01** (2010) 016 [arXiv:0909.5092] [inSPIRE].

[22] P. Hunt and S. Sarkar, *Reconstruction of the primordial power spectrum of curvature perturbations using multiple data sets*, *JCAP* **01** (2014) 025 [arXiv:1308.2317] [inSPIRE].

[23] M. Archidiacono, E. Giusarma, A. Melchiorri and O. Mena, *Dark Radiation in extended cosmological scenarios*, *Phys. Rev.* **D 86** (2012) 043509 [arXiv:1206.0109] [inSPIRE].

[24] G.-B. Zhao et al., *The clustering of galaxies in the SDSS-III Baryon Oscillation Spectroscopic Survey: weighing the neutrino mass using the galaxy power spectrum of the CMASS sample*, *Mon. Not. Roy. Astron. Soc.* **436** (2013) 2038 [arXiv:1211.3741] [inSPIRE].

[25] J.A. Vazquez, M. Bridges, Y.-Z. Ma and M.P. Hobson, *Constraints on the tensor-to-scalar ratio for non-power-law models*, *JCAP* **08** (2013) 001 [arXiv:1303.4014] [inSPIRE].

[26] K.N. Abazajian, G. Aslanyan, R. Easther and L.C. Price, *The Knotted Sky II: Does BICEP2 require a nontrivial primordial power spectrum?*, *JCAP* **08** (2014) 053 [arXiv:1403.5922] [inSPIRE].

[27] C. Cheng, Q.-G. Huang and W. Zhao, *Constraints on the extensions to the base ΛCDM model from BICEP2, Planck and WMAP*, *Sci. China Phys. Mech. Astron.* **57** (2014) 1460 [arXiv:1404.3467] [inSPIRE].

[28] A.D. Dolgov and F.L. Villante, *BBN bounds on active sterile neutrino mixing*, *Nucl. Phys.* **B 679** (2004) 261 [hep-ph/0308083] [inSPIRE].

[29] M. Cirelli, G. Marandella, A. Strumia and F. Vissani, *Probing oscillations into sterile neutrinos with cosmology, astrophysics and experiments*, *Nucl. Phys.* **B 708** (2005) 215 [hep-ph/0403158] [inSPIRE].

[30] E. Di Valentino, A. Melchiorri and O. Mena, *Dark radiation sterile neutrino candidates after Planck data*, *JCAP* **11** (2013) 018 [arXiv:1304.5981] [inSPIRE].

[31] M. Archidiacono, N. Fornengo, C. Giunti, S. Hannestad and A. Melchiorri, *Sterile neutrinos: Cosmology versus short-baseline experiments*, *Phys. Rev.* **D 87** (2013) 125034 [arXiv:1302.6720] [inSPIRE].

[32] A. Mirizzi et al., *The strongest bounds on active-sterile neutrino mixing after Planck data*, *Phys. Lett.* **B 726** (2013) 8 [arXiv:1303.5368] [inSPIRE].

[33] S. Gariazzo, C. Giunti and M. Laveder, *Light Sterile Neutrinos in Cosmology and Short-Baseline Oscillation Experiments*, *JHEP* **11** (2013) 211 [arXiv:1309.3192] [inSPIRE].

[34] M. Archidiacono, N. Fornengo, S. Gariazzo, C. Giunti, S. Hannestad et al., *Light sterile neutrinos after BICEP-2*, *JCAP* **06** (2014) 031 [arXiv:1404.1794] [inSPIRE].

[35] J. Bergström, M.C. Gonzalez-Garcia, V. Niro and J. Salvado, *Statistical tests of sterile neutrinos using cosmology and short-baseline data*, *JHEP* **10** (2014) 104 [arXiv:1407.3806] [inSPIRE].

[36] Y.-Z. Chu and M. Cirelli, *Sterile neutrinos, lepton asymmetries, primordial elements: How much of each?*, *Phys. Rev.* **D 74** (2006) 085015 [astro-ph/0608206] [inSPIRE].

[37] S. Hannestad, I. Tamborra and T. Tram, *Thermalisation of light sterile neutrinos in the early universe*, *JCAP* **07** (2012) 025 [arXiv:1204.5861] [inSPIRE].

[38] A. Mirizzi, N. Saviano, G. Miele and P.D. Serpico, *Light sterile neutrino production in the early universe with dynamical neutrino asymmetries*, *Phys. Rev.* **D 86** (2012) 053009 [arXiv:1206.1046] [INSPIRE].

[39] N. Saviano et al., *Multi-momentum and multi-flavour active-sterile neutrino oscillations in the early universe: role of neutrino asymmetries and effects on nucleosynthesis*, *Phys. Rev.* **D 87** (2013) 073006 [arXiv:1302.1200] [INSPIRE].

[40] S. Hannestad, R.S. Hansen and T. Tram, *Can active-sterile neutrino oscillations lead to chaotic behavior of the cosmological lepton asymmetry?*, *JCAP* **04** (2013) 032 [arXiv:1302.7279] [INSPIRE].

[41] S. Hannestad, R.S. Hansen and T. Tram, *How Self-Interactions can Reconcile Sterile Neutrinos with Cosmology*, *Phys. Rev. Lett.* **112** (2014) 031802 [arXiv:1310.5926] [INSPIRE].

[42] B. Dasgupta and J. Kopp, *Cosmologically Safe eV-Scale Sterile Neutrinos and Improved Dark Matter Structure*, *Phys. Rev. Lett.* **112** (2014) 031803 [arXiv:1310.6337] [INSPIRE].

[43] T. Bringmann, J. Hasenkamp and J. Kersten, *Tight bonds between sterile neutrinos and dark matter*, *JCAP* **07** (2014) 042 [arXiv:1312.4947] [INSPIRE].

[44] P. Ko and Y. Tang, *νΛMDM: A Model for Sterile Neutrino and Dark Matter Reconciles Cosmological and Neutrino Oscillation Data after BICEP2*, *Phys. Lett.* **B 739** (2014) 62 [arXiv:1404.0236] [INSPIRE].

[45] M. Archidiacono, S. Hannestad, R.S. Hansen and T. Tram, *Cosmology with self-interacting sterile neutrinos and dark matter: A pseudoscalar model*, *Phys. Rev.* **D 91** (2015) 065021 [arXiv:1404.5915] [INSPIRE].

[46] N. Saviano, O. Pisanti, G. Mangano and A. Mirizzi, *Unveiling secret interactions among sterile neutrinos with big-bang nucleosynthesis*, *Phys. Rev.* **D 90** (2014) 113009 [arXiv:1409.1680] [INSPIRE].

[47] A. Mirizzi, G. Mangano, O. Pisanti and N. Saviano, *Collisional production of sterile neutrinos via secret interactions and cosmological implications*, *Phys. Rev.* **D 91** (2015) 025019 [arXiv:1410.1385] [INSPIRE].

[48] T. Rehagen and G.B. Gelmini, *Effects of kination and scalar-tensor cosmologies on sterile neutrinos*, *JCAP* **06** (2014) 044 [arXiv:1402.0607] [INSPIRE].

[49] C.M. Ho and R.J. Scherrer, *Sterile Neutrinos and Light Dark Matter Save Each Other*, *Phys. Rev.* **D 87** (2013) 065016 [arXiv:1212.1689] [INSPIRE].

[50] P. Mukherjee and Y. Wang, *Wavelet band powers of the primordial power spectrum from CMB data*, *Astrophys. J.* **593** (2003) 38 [astro-ph/0301058] [INSPIRE].

[51] P. Mukherjee and Y. Wang, *Direct wavelet expansion of the primordial power spectrum: Results from pre-MAP CMB data*, *Astrophys. J.* **598** (2003) 779 [astro-ph/0301562] [INSPIRE].

[52] P. Mukherjee and Y. Wang, *Model-independent reconstruction of the primordial power spectrum from WMAP data*, *Astrophys. J.* **599** (2003) 1 [astro-ph/0303211] [INSPIRE].

[53] P. Mukherjee and Y. Wang, *Primordial power spectrum reconstruction*, *JCAP* **12** (2005) 007 [astro-ph/0502136] [INSPIRE].

[54] S.M. Leach, *Measuring the primordial power spectrum: Principal component analysis of the cosmic microwave background*, *Mon. Not. Roy. Astron. Soc.* **372** (2006) 646 [astro-ph/0506390].

[55] Y. Wang, D.N. Spergel and M.A. Strauss, *Cosmology in the next millennium: Combining MAP and SDSS data to constrain inflationary models*, *Astrophys. J.* **510** (1999) 20 [astro-ph/9802231] [INSPIRE].

[56] S. Hannestad, *Reconstructing the inflationary power spectrum from CMBR data*, *Phys. Rev.* **D 63** (2001) 043009 [astro-ph/0009296] [inSPIRE].

[57] D.K. Hazra, A. Shafieloo and G.F. Smoot, *Reconstruction of broad features in the primordial spectrum and inflaton potential from Planck*, *JCAP* **12** (2013) 035 [arXiv:1310.3038] [inSPIRE].

[58] Y. Wang and G. Mathews, *A measurement of the primordial power spectrum from Maxima and Boomerang data*, *Astrophys. J.* **573** (2002) 1 [astro-ph/0011351] [inSPIRE].

[59] S. Bridle, A. Lewis, J. Weller and G. Efstathiou, *Reconstructing the primordial power spectrum*, *Mon. Not. Roy. Astron. Soc.* **342** (2003) L72 [astro-ph/0302306].

[60] S. Hannestad, *Reconstructing the primordial power spectrum - A new algorithm*, *JCAP* **04** (2004) 002 [astro-ph/0311491] [inSPIRE].

[61] M. Bridges, A. Lasenby and M. Hobson, *A bayesian analysis of the primordial power spectrum*, *Mon. Not. Roy. Astron. Soc.* **369** (2006) 1123 [astro-ph/0511573].

[62] WMAP collaboration, D.N. Spergel et al., *Wilkinson Microwave Anisotropy Probe (WMAP) three year results: implications for cosmology*, *Astrophys. J. Suppl.* **170** (2007) 377 [astro-ph/0603449] [inSPIRE].

[63] M. Bridges, A. Lasenby and M. Hobson, *WMAP 3-year primordial power spectrum*, *Mon. Not. Roy. Astron. Soc.* **381** (2007) 68 [astro-ph/0607404].

[64] M. Bridges, F. Feroz, M. Hobson and A. Lasenby, *Bayesian optimal reconstruction of the primordial power spectrum*, *Mon. Not. Roy. Astron. Soc.* **400** (2009) 1075 [arXiv:0812.3541].

[65] D.K. Hazra, A. Shafieloo, G.F. Smoot and A.A. Starobinsky, *Ruling out the power-law form of the scalar primordial spectrum*, *JCAP* **06** (2014) 061 [arXiv:1403.7786] [inSPIRE].

[66] C. Sealfon, L. Verde and R. Jimenez, *Smoothing spline primordial power spectrum reconstruction*, *Phys. Rev.* **D 72** (2005) 103520 [astro-ph/0506707] [inSPIRE].

[67] L. Verde and H.V. Peiris, *On Minimally-Parametric Primordial Power Spectrum Reconstruction and the Evidence for a Red Tilt*, *JCAP* **07** (2008) 009 [arXiv:0802.1219] [inSPIRE].

[68] H.V. Peiris and L. Verde, *The Shape of the Primordial Power Spectrum: A Last Stand Before Planck*, *Phys. Rev.* **D 81** (2010) 021302 [arXiv:0912.0268] [inSPIRE].

[69] R. Hlozek et al., *The Atacama Cosmology Telescope: a measurement of the primordial power spectrum*, *Astrophys. J.* **749** (2012) 90 [arXiv:1105.4887] [inSPIRE].

[70] C. Gauthier and M. Bucher, *Reconstructing the primordial power spectrum from the CMB*, *JCAP* **10** (2012) 050 [arXiv:1209.2147] [inSPIRE].

[71] R. de Putter, E.V. Linder and A. Mishra, *Inflationary Freedom and Cosmological Neutrino Constraints*, *Phys. Rev.* **D 89** (2014) 103502 [arXiv:1401.7022] [inSPIRE].

[72] B. Hu, J.-W. Hu, Z.-K. Guo and R.-G. Cai, *Reconstruction of the primordial power spectra with Planck and BICEP2 data*, *Phys. Rev.* **D 90** (2014) 023544 [arXiv:1404.3690] [inSPIRE].

[73] LSND collaboration, A. Aguilar-Arevalo et al., *Evidence for neutrino oscillations from the observation of anti-neutrino(electron) appearance in a anti-neutrino(muon) beam*, *Phys. Rev.* **D 64** (2001) 112007 [hep-ex/0104049] [inSPIRE].

[74] J.N. Abdurashitov et al., *Measurement of the response of a Ga solar neutrino experiment to neutrinos from an Ar-37 source*, *Phys. Rev.* **C 73** (2006) 045805 [nucl-ex/0512041] [inSPIRE].

[75] M. Laveder, *Unbound neutrino roadmaps*, *Nucl. Phys. Proc. Suppl.* **168** (2007) 344.

[76] C. Giunti and M. Laveder, *Short-Baseline Active-Sterile Neutrino Oscillations?*, *Mod. Phys. Lett.* **A 22** (2007) 2499 [hep-ph/0610352] [INSPIRE].

[77] M.A. Acero, C. Giunti and M. Laveder, *Limits on nu(e) and anti-nu(e) disappearance from Gallium and reactor experiments*, *Phys. Rev.* **D 78** (2008) 073009 [arXiv:0711.4222] [INSPIRE].

[78] C. Giunti and M. Laveder, *Statistical Significance of the Gallium Anomaly*, *Phys. Rev.* **C 83** (2011) 065504 [arXiv:1006.3244] [INSPIRE].

[79] T. Mueller et al., *Improved Predictions of Reactor Antineutrino Spectra*, *Phys. Rev.* **C 83** (2011) 054615 [arXiv:1101.2663] [INSPIRE].

[80] G. Mention et al., *The Reactor Antineutrino Anomaly*, *Phys. Rev.* **D 83** (2011) 073006 [arXiv:1101.2755] [INSPIRE].

[81] P. Huber, *On the determination of anti-neutrino spectra from nuclear reactors*, *Phys. Rev.* **C 84** (2011) 024617 [*Erratum ibid.* **C 85** (2012) 029901] [arXiv:1106.0687] [INSPIRE].

[82] S.M. Bilenky, C. Giunti and W. Grimus, *Phenomenology of neutrino oscillations*, *Prog. Part. Nucl. Phys.* **43** (1999) 1 [hep-ph/9812360] [INSPIRE].

[83] M.C. Gonzalez-Garcia and M. Maltoni, *Phenomenology with Massive Neutrinos*, *Phys. Rept.* **460** (2008) 1 [arXiv:0704.1800] [INSPIRE].

[84] K.N. Abazajian et al., *Light Sterile Neutrinos: A White Paper*, arXiv:1204.5379 [INSPIRE].

[85] M.C. Gonzalez-Garcia, M. Maltoni, J. Salvado and T. Schwetz, *Global fit to three neutrino mixing: critical look at present precision*, *JHEP* **12** (2012) 123 [arXiv:1209.3023] [INSPIRE].

[86] G. Bellini, L. Ludhova, G. Ranucci and F.L. Villante, *Neutrino oscillations*, *Adv. High Energy Phys.* **2014** (2014) 191960 [arXiv:1310.7858] [INSPIRE].

[87] F. Capozzi et al., *Status of three-neutrino oscillation parameters, circa 2013*, *Phys. Rev.* **D 89** (2014) 093018 [arXiv:1312.2878] [INSPIRE].

[88] M. Gonzalez-Garcia, M. Maltoni and T. Schwetz, NuFIT, http://www.nu-fit.org/.

[89] J. Kopp, M. Maltoni and T. Schwetz, *Are there sterile neutrinos at the eV scale?*, *Phys. Rev. Lett.* **107** (2011) 091801 [arXiv:1103.4570] [INSPIRE].

[90] C. Giunti and M. Laveder, *3+1 and 3+2 Sterile Neutrino Fits*, *Phys. Rev.* **D 84** (2011) 073008 [arXiv:1107.1452] [INSPIRE].

[91] C. Giunti and M. Laveder, *Status of 3+1 Neutrino Mixing*, *Phys. Rev.* **D 84** (2011) 093006 [arXiv:1109.4033] [INSPIRE].

[92] C. Giunti and M. Laveder, *Implications of 3+1 Short-Baseline Neutrino Oscillations*, *Phys. Lett.* **B 706** (2011) 200 [arXiv:1111.1069] [INSPIRE].

[93] J.M. Conrad, C.M. Ignarra, G. Karagiorgi, M.H. Shaevitz and J. Spitz, *Sterile Neutrino Fits to Short Baseline Neutrino Oscillation Measurements*, *Adv. High Energy Phys.* **2013** (2013) 163897 [arXiv:1207.4765] [INSPIRE].

[94] J. Kopp, P.A.N. Machado, M. Maltoni and T. Schwetz, *Sterile Neutrino Oscillations: The Global Picture*, *JHEP* **05** (2013) 050 [arXiv:1303.3011] [INSPIRE].

[95] C. Giunti, M. Laveder, Y.F. Li and H.W. Long, *Pragmatic View of Short-Baseline Neutrino Oscillations*, *Phys. Rev.* **D 88** (2013) 073008 [arXiv:1308.5288] [INSPIRE].

[96] PLANCK collaboration, P.A.R. Ade et al., *Planck 2013 results. XVI. Cosmological parameters*, *Astron. Astrophys.* **571** (2014) A16 [arXiv:1303.5076] [INSPIRE].

[97] M. Archidiacono, N. Fornengo, C. Giunti and A. Melchiorri, *Testing 3+1 and 3+2 neutrino mass models with cosmology and short baseline experiments*, *Phys. Rev.* **D 86** (2012) 065028 [arXiv:1207.6515] [INSPIRE].

[98] S. Gariazzo, C. Giunti and M. Laveder, *Cosmological Invisible Decay of Light Sterile Neutrinos*, arXiv:1404.6160 [INSPIRE].

[99] G. Mangano et al., *Relic neutrino decoupling including flavor oscillations*, *Nucl. Phys.* **B 729** (2005) 221 [hep-ph/0506164] [INSPIRE].

[100] M. Archidiacono, E. Giusarma, S. Hannestad and O. Mena, *Cosmic dark radiation and neutrinos*, *Adv. High Energy Phys.* **2013** (2013) 191047 [arXiv:1307.0637] [INSPIRE].

[101] J. Lesgourgues and S. Pastor, *Neutrino cosmology and Planck*, *New J. Phys.* **16** (2014) 065002 [arXiv:1404.1740] [INSPIRE].

[102] F. Fritsch and R. Carlson, *Monotone Piecewise Cubic Interpolation*, *SIAM J. Numer. Anal.* **17** (1980) 238.

[103] J.B. Fred Fritsch, *A Method for Constructing Local Monotone Piecewise Cubic Interpolants*, *SIAM J. Sci. Stat. Comput.* **5** (1984) 300.

[104] D. Larson et al., *Seven-Year Wilkinson Microwave Anisotropy Probe (WMAP) Observations: Power Spectra and WMAP-Derived Parameters*, *Astrophys. J. Suppl.* **192** (2011) 16 [arXiv:1001.4635] [INSPIRE].

[105] A. Lewis and S. Bridle, *Cosmological parameters from CMB and other data: A Monte Carlo approach*, *Phys. Rev.* **D 66** (2002) 103511 [astro-ph/0205436] [INSPIRE].

[106] A. Lewis, A. Challinor and A. Lasenby, *Efficient computation of CMB anisotropies in closed FRW models*, *Astrophys. J.* **538** (2000) 473 [astro-ph/9911177] [INSPIRE].

[107] BICEP2 collaboration, P.A.R. Ade et al., *Detection of B-Mode Polarization at Degree Angular Scales by BICEP2*, *Phys. Rev. Lett.* **112** (2014) 241101 [arXiv:1403.3985] [INSPIRE].

[108] PLANCK collaboration, P.A.R. Ade et al., *Planck 2013 results. XV. CMB power spectra and likelihood*, *Astron. Astrophys.* **571** (2014) A15 [arXiv:1303.5075] [INSPIRE].

[109] J. Dunkley et al., *The Atacama Cosmology Telescope: likelihood for small-scale CMB data*, *JCAP* **07** (2013) 025 [arXiv:1301.0776] [INSPIRE].

[110] K.T. Story et al., *A Measurement of the Cosmic Microwave Background Damping Tail from the 2500-square-degree SPT-SZ survey*, *Astrophys. J.* **779** (2013) 86 [arXiv:1210.7231] [INSPIRE].

[111] A.G. Riess et al., *A 3% Solution: Determination of the Hubble Constant with the Hubble Space Telescope and Wide Field Camera 3*, *Astrophys. J.* **730** (2011) 119 [*Erratum ibid.* **732** (2011) 129] [arXiv:1103.2976] [INSPIRE].

[112] PLANCK collaboration, P.A.R. Ade et al., *Planck 2013 results. XX. Cosmology from SunyaevZeldovich cluster counts*, *Astron. Astrophys.* **571** (2014) A20 [arXiv:1303.5080] [INSPIRE].

[113] M. Kilbinger et al., *CFHTLenS: Combined probe cosmological model comparison using 2D weak gravitational lensing*, *Monthly Notices of the Royal Astronomical Society* **430** (2013) 2200 [arXiv:1212.3338] [INSPIRE].

[114] C. Heymans et al., *CFHTLenS tomographic weak lensing cosmological parameter constraints: Mitigating the impact of intrinsic galaxy alignments*, *Mon. Not. Roy. Astron. Soc.* **432** (2013) 2433 [arXiv:1303.1808] [INSPIRE].

[115] PLANCK collaboration, R. Adam et al., *Planck intermediate results. XXX. The angular power spectrum of polarized dust emission at intermediate and high Galactic latitudes*, arXiv:1409.5738 [INSPIRE].

[116] W.H. Press, S.A. Teukolsky, W.T. Vetterling and B.P. Flannery, *Numerical Recipes 3rd Edition: The Art of Scientific Computing*, third edition, Cambridge University Press, New York, U.S.A. (2007).